

Femtosecond laser direct patterning of sensing materials toward flexible integration of micronanosensors

Li Guo,¹ Hong Xia,¹ Hui-Tao Fan,¹ Yong-Lai Zhang,¹ Qi-Dai Chen,¹
Tong Zhang,^{1,3} and Hong-Bo Sun^{1,2,4}

¹State Key Laboratory on Integrated Optoelectronics, College of Electronic Science and Engineering,
Jilin University, 2699 Qianjin Street, Changchun 130012, China

²College of Physics, Jilin University, 119 Jiefang Road, Changchun 130023, China

³zhangtong@jlu.edu.cn

⁴hbsun@jlu.edu.cn

Received January 25, 2010; revised April 10, 2010; accepted April 15, 2010;
posted April 22, 2010 (Doc. ID 123226); published May 14, 2010

Reported is femtosecond laser direct patterning of sensing materials toward flexible integration of micronanosensors (FIMS), meaning the capability to fabricate multiple functional sensors of smaller size on a nonflat surface of a substrate that is not limited to silicon. As a representative example, a photosensitive SnO₂ colloidal solution (sol) was developed, from which complex micronanostructures were written via a two-photon absorption process. After thermal decomposition of organic components, the patterned SnO₂ microsensors responded to relative humidity (RH) with a variation range of 5 orders of magnitude. FIMS would open a new door for miniaturization of micronanosensors expected in intelligent microsystems. © 2010 Optical Society of America

OCIS codes: 160.6060, 220.4241.

Microsensors exhibit unique advantages such as reduction in system size, weight, and cost, improvement in response time and reliability, and ease of integration of sensing elements with supporting circuitry for constant heating power supplies, multiplexers, signal conditioning, analog-to-digital conversion, and micro-hot-plates [1]. Generally, a microsensor is created by pasting a continuous semiconductor oxide film on a pair of lithographically produced metal comblike electrodes, and the portion of the film between the two fingers fulfills the effective sensing function [2,3]. The planar-lithography-dominated fabrication process and the microsensors it produces do not satisfy the increasing demand from intelligent microsystem or nanorobot development [4,5], for which multiple sensing elements of smaller size, attachable to nonflat substrates of nonsilicon materials are needed. The capability to incorporate sensing elements on arbitrarily shaped surfaces of any material, which here we call flexible integration of micronanosensors (FIMS), is desired, but remains a technical challenge. In this Letter, we solve the problem by femtosecond laser direct nanopatterning [6–8] of sensing materials, for which the key functional material extensively used as gas sensors, tin dioxide (SnO₂), was chosen as an example [9,10]. The idea was encouraged by the pioneering works on prototyping sol-gel-based metal chelates, for example, colloidal solutions (sols) of Al₂O₃, Al₂O₃-SiO₂, and SnO₂ by Zhao *et al.* [11,12] and TiO₂ by Passinger *et al.* [13] for 3D photonic crystals. A femtosecond laser is not indispensable for FIMS but is found helpful to reduce the line width and pattern size and improve the structural complexity and functional controllability of sensing devices.

Figure 1(a) illustrates the reaction equation for preparing the photosensitive SnO₂ sol. Tin dichloride was implemented as the precursory material, acetylacetonate (AcAc) as a chemical modifier, and 2-methoxyethanol as the solvent. Pentaerythritol triacrylate (PETA) was chosen as the stability reagent. Experimentally, SnCl₂

(4.5 g) was dissolved in 2-methoxyethanol (20 ml) and stirred for 1 h at 50°C. After cooling down to room temperature, AcAc was mixed in terms of the molar ratio Sn : AcAc = 1 : 3 and the mixture was stirred for 3 h at room temperature. PETA (2 g) was then added to increase the stability and viscosity of the sol. The as-obtained SnO₂ sol was used for further processing. The SnO₂ sol was spin-coated on a quartz wafer and further evaporated into a gel film for absorption characterization. The optical absorption of the SnO₂ gel films varied before and after UV irradiation for 30 min [Fig. 1(b)]. The obvious absorption band peaking at around 302 nm is considered to originate from the $\pi - \pi^*$ electronic transition of the chelate ring [14], indicating that AcAc formed a chelate ring with tin ions. When the SnO₂ gel film was exposed to UV light,

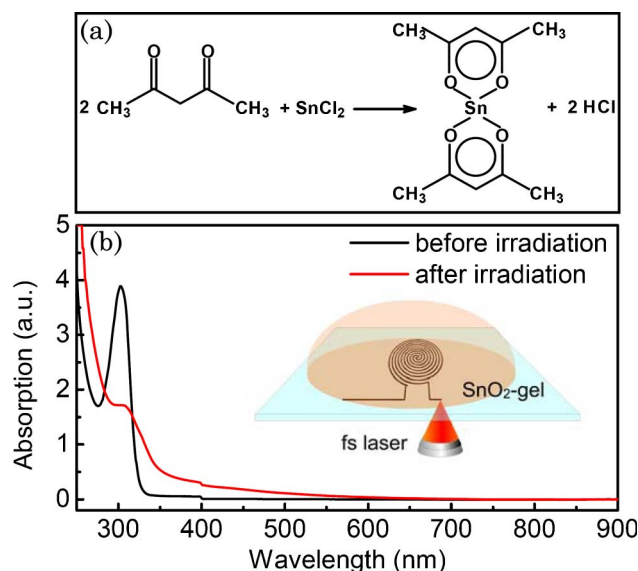


Fig. 1. (Color online) (a) Fabrication process of micronanostructured SnO₂. (a) Synthetic equation of photosensitive SnO₂ sol. (b) Optical absorption spectra of as-prepared SnO₂ gels before and after UV irradiation. Inset, scheme for femtosecond laser processing.

the intensity of the absorption band decreased drastically owing to the breakdown of the (C–C) and (C–O) bonds in the chelate ring. This in turn reduces their solubility in organic solutions significantly [14]. The bond breaking, or molecular fragmentation, responsible for the photo-degradation can also be induced by two-photon or multi-photon excitation when SnO_2 gel is exposed to femto-second laser pulses of near-infrared wavelength. As a result, the exposed region of the SnO_2 gel behaves as insoluble in organic solvents such as acetone. The locus of sedimentation, following the trace of preprogrammed patterns, may be shaped into 2D or 3D patterns [inset of Fig. 1(b)].

For laser micronanofabrication, a drop of as-synthesized SnO_2 sol was dripped on a cover glass as the substrate. Pulses from a femtosecond laser oscillator (Tsunami, Spectra Physics) of 780 nm central wavelength, 120 fs pulse duration, and 80 MHz repetition rate, were tightly focused by a 100 \times oil immersion objective lens with a high numerical aperture (NA) of 1.35. The focal spot of the laser beam was scanned laterally by steering a two-galvano-mirror set and was vertically moved along the optical axis by a piezo stage. During the writing procedure, 16–20 mW laser power measured before the objective lens, 100 nm scanning step length, and 600 μs exposure duration for each voxel were adopted. It is worth pointing out that after the SnO_2 sol is dripped onto the glass, waiting for around 10 min is necessary, by which time part of the solvent was evaporated, making the SnO_2 sol a wet gel. Herein, PETA behaves as a framework filling because of its help in stabilizing the formed micronanostructures. After the writing, the entire structure was rinsed with acetone for 1 h to remove the unsolidified gel, and well-defined structures were achieved. Crystallized SnO_2 microstructures were finally obtained after thermal decomposition of the organic components. As a typical example, double wire loops were fabricated through direct laser writing from SnO_2 gel [Fig. 2(a)]. The minimized width of wires is around 400 nm. After a thermal treatment of the patterns at 500°C in atmosphere for 2 h, the width of the SnO_2 double wire loops shrank to approximately 150 nm [Fig. 2(b)], owing to the removal of organic components. With such a high resolution, even complex patterns such as a Jilin University badge were easily created, from which the resolution improvement following calcination was confirmed.

As expected, the fabrication strategy was applicable to not only 2D patterns, but also 3D structures. For the 3D prototyping, use of two-photon absorption, permitting deeper penetration of the light beam into the solution without significant power loss because of the negligible linear absorption at the near-infrared wavelength, is critical. As shown in Figs. 3(a) and 3(b), a typical 3D cage consisting of a wire network was attained. The well-defined 3D shape was preserved without distortion after being calcined at 500°C in atmosphere for 2 h, showing that the mechanical strength of the network is large enough for the structure to self-support [insets of Figs. 3(a) and 3(b)]. Further x-ray diffraction study shows that the nanostructured SnO_2 was highly crystallized. The whole set of diffraction peaks were attributed

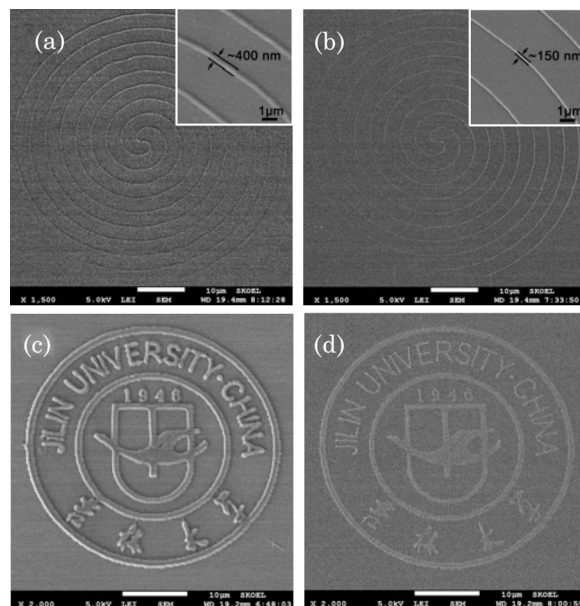


Fig. 2. SEM images of 2D SnO_2 micronanostructures. Double line loops (a) before calcination, and (b) after calcination. Insets, magnified images. (c) Badge of Jilin University before calcination and (d) after calcination.

to the tetragonal rutile structure without phases of impurities [Fig. 3(c)].

Well-defined shapes alone are still insufficient for device functions, for which a particular material capability has to be involved. As an oxygen-deficient *n*-type semiconductor, SnO_2 film has been used in resistance sensors. Therefore, the sensitivity of the wire electric conductivity to the ambient gases is critical for its prospect in microsensors. As a test, SnO_2 wire of about 700 nm in diameter and 123 μm in length was direct written between two Au electrodes (100 nm in thickness) [Fig. 4(a)]. The I–V curve exhibits good linear dependence, from which the specific resistance of the wire was calculated to be 5500 $\Omega\text{ cm}$ (the section of the wire was estimated as approximately a square), nearly 2 orders of magnitude higher than the bulk SnO_2 ,

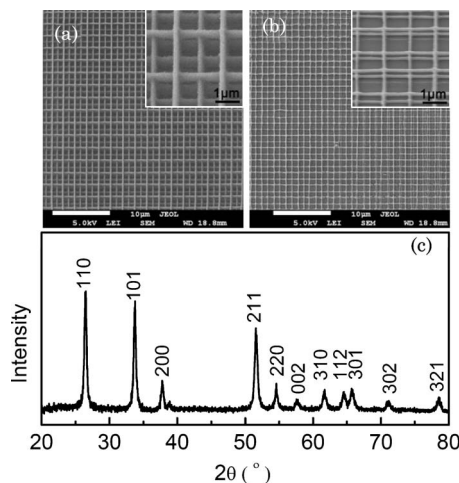


Fig. 3. SEM images of 3D SnO_2 cage structures. (a) 3D cage before calcination and (b) after calcination. Insets, magnified images. (c) Wide-angle x-ray diffraction curves of the SnO_2 after calcination.

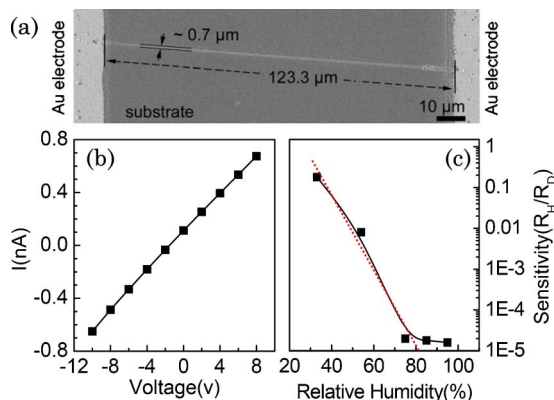


Fig. 4. (Color online) (a) Scanning electron microscopy image of a SnO_2 nanowire between two Au electrodes. (b) I-V curve of the SnO_2 nanowire. (c) Dependence of resistance on RH of the SnO_2 nanowire.

$93 \Omega \text{ cm}$ at room temperature. This should result from the formation of a porous construction of nanocrystallites, as a result of crystal growth accompanied evaporation of the organic composition. Such structures should be feasible to absorb ambient molecules so that the wire resistance becomes sensitive to the ambient gases, as for the simplest case, water. Figure 3(c) shows the response sensitivity (R_H/R_D , the ratio of resistance in humidity to that in dry air) of SnO_2 wire at room temperature. Notably, the resistance decreases with the increase of relative humidity (RH) in air. The range of the variety is as wide as 5 orders of magnitude. In the range of 30%–80% RH, the logarithmic resistance ratio shows typical linear dependence on RH, indicating its excellent sensitivity. The mechanism has been proposed to be the significant change of surface conductivity in the presence of water molecules [15,16]. On the surface, outward positive and negative ions are not shielded with their counter ions. The positive ions form an acceptor level just below the bottom of the conduction band, and the negative ions form a donor level near top of the valence band. Especially, for *n*-type semiconductors, electrons at the surface transfer to the acceptor level preferentially, forming a negative space charge region, which prevents the electrons from transferring to the acceptor level. Thus an electronic potential barrier was finally formed in the surface, giving birth to an electronic depletion layer on the surface. All of the above results would cause a large resistance. Generally, water molecules adsorbed on the surface could provide a surface donor level that would inject electrons to the surface of the semiconductor. As shown in the reaction, $\text{H}_2\text{O}(\text{g}) + \text{O}^-_{\text{ad}} \rightarrow 2\text{OH}^-_{\text{ad}} + \text{e}$. After re-

leasing an electron, the resistance decreases significantly with the barrier's decline. Therefore, our micronanostructured SnO_2 shows a sensitive response to RH.

In summary, we have proposed the flexible integration of microsensors (FIMS) by direct patterning sensing materials via femtosecond laser processing. As a simple example, a SnO_2 nanowire created between two Au electrodes was used as a humidity microsensors, which exhibits a five-order change of the electric resistance versus the humidity variation. The novel nano-processing mechanism of laser-induced molecular fragmentation exhibits great technological potential for fabrication and integration of various electronic, mechanical, and electronic miniaturized devices, including sensors.

This research was supported by NSFC under grants 60978048, 60977056, 60525412, and 90923037.

References

1. I. Simon, N. Bârsan, M. Bauer, and U. Weimar, *Sens. Actuators. B* **73**, 1 (2001).
2. Q. Qi, T. Zhang, Q. Yu, R. Wang, Y. Zeng, L. Liu, and H. B. Yang, *Sens. Actuators. B* **133**, 638 (2008).
3. M. Graf, D. Barlettino, S. Taschini, C. Hagleitner, A. Hierlemann, and H. Baltes, *Anal. Chem.* **76**, 4437 (2004).
4. Y.-S. Lee, K.-D. Song, J.-S. Huh, W.-Y. Chung, and D.-D. Lee, *Sens. Actuators. B* **108**, 292 (2005).
5. A. Hierlemann, O. Brand, C. Hagleitner, and H. Baltes, *Proc. IEEE*, **91**, 839 (2003).
6. H. Xia, W.-Y. Zhang, F.-F. Wang, D. Wu, X.-W. Liu, L. Chen, Q.-D. Chen, Y.-G. Ma, and H.-B. Sun, *Appl. Phys. Lett.* **95**, 083118 (2009).
7. D. Wu, Q.-D. Chen, L.-G. Niu, J.-N. Wang, J. Wang, R. Wang, H. Xia, and H.-B. Sun, *Lab. Chip.* **9**, 2391 (2009).
8. J. Wang, H. Xia, B.-B. Xu, L.-G. Niu, D. Wu, Q.-D. Chen, and H.-B. Sun, *Opt. Lett.* **34**, 581 (2009).
9. Q. Kuang, C. S. Lao, Z. L. Wang, Z. X. Xie, and L. S. Zheng, *J. Am. Chem. Soc.* **129**, 6070 (2007).
10. X. Song, Q. Qi, T. Zhang, and C. Wang, *Sens. Actuators. B* **138**, 368 (2009).
11. W. Zhang, G. Zhao, and Z. Chen, *Mater. Sci. Eng. B* **99**, 168 (2003).
12. Y. Li, G. Zhao, W. Zhang, and Y. Chen, *Surf. Interface Anal.* **38**, 1328 (2006).
13. S. Passinger, M. S. M. Saifullah, C. Reinhardt, K. R. V. Subramanian, B. N. Chichkov, and M. E. Welland, *Adv. Mater.* **19**, 1218 (2007).
14. N. Tohge, K. Shinmou, and T. Minami, *J. Sol-Gel Sci. Technol.* **2**, 581 (1994).
15. T. Seiyama, ed., *Chemical Sensor Technology* (Kodansha, 1989), Vol. 2, pp. 133–149.
16. V. A. Henrich and P. A. Cox, *The Surface Science of Metal Oxides* (Cambridge Univ. Press, 1994).